



Precise determination of the $B_s^0-\bar{B}_s^0$ oscillation frequency

LHCb collaboration[†]

Abstract

Mesons comprising a beauty quark and a strange quark can oscillate between particle (B_s^0) and antiparticle (\bar{B}_s^0) flavour eigenstates, with a frequency given by the mass difference between heavy and light mass eigenstates, Δm_s . Here we present a measurement of Δm_s using $B_s^0 \rightarrow D_s^- \pi^+$ decays produced in proton-proton collisions collected with the LHCb detector at the Large Hadron Collider. The oscillation frequency is found to be $\Delta m_s = 17.7683 \pm 0.0051 \pm 0.0032 \text{ ps}^{-1}$, where the first uncertainty is statistical and the second systematic. This measurement improves upon the current Δm_s precision by a factor of two. We combine this result with previous LHCb measurements to determine $\Delta m_s = 17.7656 \pm 0.0057 \text{ ps}^{-1}$, which is the legacy measurement of the original LHCb detector.

Published in Nature Physics 18, (2022) 1

© 2022 CERN for the benefit of the LHCb collaboration. CC BY 4.0 licence.

[†]Authors are listed at the end of this paper.

Neutral mesons with strange, charm or beauty quantum numbers can mix with their antiparticles, as these quantum numbers are not conserved by the weak interaction. The neutral meson comprising an antibeauty quark and a strange quark, the B_s^0 meson, and its antiparticle, the \bar{B}_s^0 meson, are one such example. In the B_s^0 – \bar{B}_s^0 system, the observed particle and antiparticle states are linear combinations of the heavy (H) and light (L) mass eigenstates. The mass eigenstates have masses m_H and m_L and decay widths Γ_H and Γ_L [1]. As a consequence, the B_s^0 – \bar{B}_s^0 system oscillates with a frequency given by the mass difference, $\Delta m_s = m_H - m_L$. This oscillation frequency is an important parameter of the Standard Model of particle physics. In combination with the B^0 – \bar{B}^0 oscillation frequency, Δm_d , it provides a powerful constraint on the Cabibbo–Kobayashi–Maskawa quark-mixing matrix [2–6]. A precise measurement of Δm_s is also required to reduce the systematic uncertainty associated with measurements of matter-antimatter differences in the B_s^0 – \bar{B}_s^0 system [7].

In this paper, we present a measurement of Δm_s using B_s^0 mesons that decay to a charmed-strange D_s^- meson and a pion, $B_s^0 \rightarrow D_s^- \pi^+$, and the decays with opposite charge, $\bar{B}_s^0 \rightarrow D_s^+ \pi^-$. We refer to both charge combinations as $B_s^0 \rightarrow D_s^- \pi^+$ throughout the paper, and similarly for decays of the D_s^- meson. The measurement is performed using data collected between 2015 and 2018, denoted Run 2 of the Large Hadron Collider (LHC), corresponding to an integrated luminosity of 6 fb^{-1} of proton-proton (pp) collisions at a centre-of-mass energy of 13 TeV.

The first measurement in which the significance of the observed B_s^0 – \bar{B}_s^0 oscillation signal exceed five standard deviations was obtained by the CDF collaboration [8]. More recently, the LHCb collaboration has performed several measurements of Δm_s using data collected at the LHC: a measurement using $B_s^0 \rightarrow D_s^- \pi^+$ decays [9]; two measurements using $B_s^0 \rightarrow J/\psi K^+ K^-$ decays [10, 11]; and a measurement using $B_s^0 \rightarrow D_s^\mp \pi^\pm \pi^\pm \pi^\mp$ decays [12]. Theoretical predictions for Δm_s are available [6, 13–17], with the most precise prediction in Ref. [18]. The prediction is consistent with but significantly less precise than existing experimental results.

The $B_s^0 \rightarrow D_s^- \pi^+$ decay-time distribution, in the absence of detector effects, can be written as

$$P(t) \sim e^{-\Gamma_s t} \left[\cosh \left(\frac{\Delta\Gamma_s t}{2} \right) + C \cdot \cos(\Delta m_s t) \right], \quad (1)$$

where $\Gamma_s = (\Gamma_H + \Gamma_L)/2$ is the B_s^0 meson decay width and $\Delta\Gamma_s = \Gamma_H - \Gamma_L$ is the decay-width difference between the heavy and light mass eigenstates. The parameter C takes the value $C = 1$ for unmixed decays, *i.e.* $B_s^0 \rightarrow D_s^- \pi^+$, and $C = -1$ for decays in which the initially produced meson mixed into its antiparticle before decaying, *i.e.* $B_s^0 \rightarrow \bar{B}_s^0 \rightarrow D_s^+ \pi^-$. The mixed decay is referred to as $\bar{B}_s^0 \rightarrow D_s^- \pi^+$ throughout the paper. The mass difference Δm_s corresponds to a frequency in natural units, and is measured in inverse picoseconds.

The LHCb detector [19, 20] is designed to study the decays of beauty and charm hadrons produced in pp collisions at the LHC. It instruments a region around the proton beam axis, covering the polar angles between 10 and 250 mrad, in which approximately a quarter of the b -hadron decay products are fully contained. The detector includes a high-precision tracking system with a dipole magnet, providing measurements of the momentum and decay-vertex position of particles. Different types of charged particles are distinguished using information from two ring-imaging Cherenkov detectors, a calorimeter and a muon system.

Simulated samples of $B_s^0 \rightarrow D_s^- \pi^+$ decays and data control samples are used to verify

the analysis procedure and to study systematic effects. The simulation provides a detailed model of the experimental conditions, including the pp collision, the decays of the particles produced, their final-state radiation and the response of the detector. Simulated samples are corrected for residual differences in relevant kinematic distributions to improve the agreement with data. The software used is described in Refs. [21–26].

The B_s^0 mesons travel a macroscopic distance at LHC energies (on average 1 cm) before decaying and are significantly heavier than most other particles produced directly in pp collisions. Thus their decay products have significant displacement relative to the pp collision point, and a larger momentum transverse to the beam axis, compared to other particles. The candidate selection exploits these fundamental properties. Two fast real-time selections use partial detector information to reject LHC bunch crossings likely to be incompatible with the presence of the signal, before a third selection uses fully aligned and calibrated data in real time to reconstruct and select topologies consistent with the signal [27]. Selected collisions are recorded to permanent storage. All but the first real-time selection are based on multivariate classifiers. Two subsequent selections fully reconstruct the decays with the D_s^- meson reconstructed in both $K^-K^+\pi^-$ and $\pi^-\pi^+\pi^-$ final states. After the real-time stages, the initial ‘offline’ selection is based on a data range in track kinematic quantities and displacement relative to the pp collision point that favours signal, followed by a multivariate classifier trained on properties of the full signal decay. These selections sequentially improve the signal purity of the sample to the final value of 84%, which is optimised using simulation to maximize the product of signal significance and signal efficiency. This criterion gives the optimal sensitivity to the oscillation frequency.

The remaining sources of background after selection consist of: random track combinations (combinatorial background); $B_s^0 \rightarrow D_s^{*-}\pi^+$ decays, where the photon from the $D_s^{*-} \rightarrow D_s^-\gamma$ decay is not reconstructed; and contributions from b -hadron decays with similar topologies to the signal, namely $B^0 \rightarrow D^-\pi^+$, $\bar{A}_b^0 \rightarrow \bar{A}_c^-\pi^+$ and $B_s^0 \rightarrow D_s^\mp K^\pm$ decays. The decays with similar topology are suppressed by applying kinematic vetoes and additional particle identification requirements.

In order to measure Δm_s , a $B_s^0 \rightarrow D_s^-\pi^+$ decay time distribution is first constructed in the absence of background. This is achieved by performing an unbinned two-dimensional likelihood fit to the observed $D_s^-\pi^+$ and $K^-K^+\pi^-$ or $\pi^-\pi^+\pi^-$ invariant-mass distributions. This fit is used to determine the signal yield and a set of weights [28] used to statistically subtract the background in the subsequent fit to the decay-time distribution. The invariant mass distributions of the selected decays are shown in Fig. 1. The non peaking contribution in the combinatorial background distribution, visible in Fig. 1 (right), is due to events in which a fake D_s^- candidate is produced from a combination of random tracks. The peaking contribution is due to genuine D_s^- candidates combined with a random track resulting in a fake B_s^0 candidate.

The probability density functions describing the signal and background invariant mass distributions are obtained using a mixture of control samples in data and simulation. The $D_s^-\pi^+$ and $K^-K^+\pi^-$ or $\pi^-\pi^+\pi^-$ invariant-mass signal shapes are described by the sum of a Hypatia [29] and Johnson S_U [30] functions. The combinatorial background contribution for both invariant-mass distributions is described by an exponential function in each with parameters determined in the fit. The $B^0 \rightarrow D^-\pi^+$, $\bar{A}_b^0 \rightarrow \bar{A}_c^-\pi^+$ or $B_s^0 \rightarrow D_s^\mp K^\pm$ background components constitute less than 2% of the signal yield and are accounted for in the fit to the invariant mass distributions using yields obtained from known branching

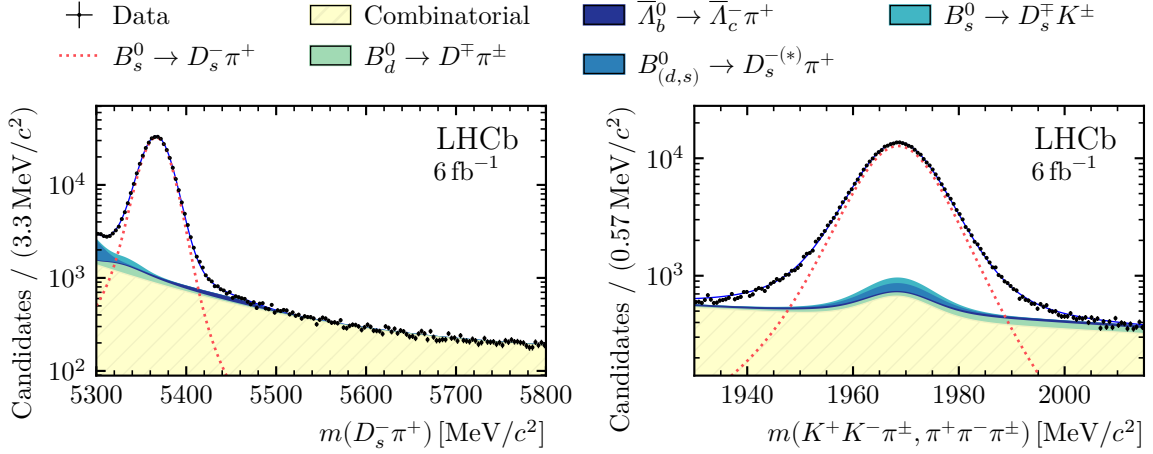


Figure 1: **Invariant-mass distributions.** Distributions of the (left) $D_s^- \pi^+$, and (right) $K^+ K^- \pi^\pm$ or $\pi^+ \pi^- \pi^\pm$ invariant mass for the selected candidates, $m(D_s^- \pi^+)$ and $m(K^+ K^- \pi^\pm, \pi^+ \pi^- \pi^\pm)$, respectively. The mass fit described in the text is overlaid. The different contributions are shown as coloured areas (for background) or by dashed lines (for signal). The vertical bars, typically visible only in regions with low numbers of candidates, correspond to the statistical uncertainty on the number of observed candidates in each bin. The horizontal bin width is indicated on the vertical axis legend.

fractions and relative efficiencies, as determined from simulated samples, which are weighted to account for differences between data and simulation. The $B^0 \rightarrow D_s^- \pi^+$ and $B_s^0 \rightarrow D_s^{*-} \pi^+$ background components are also obtained from simulated samples and included in the mass fit. The combined $B^0 \rightarrow D_s^- \pi^+$ and $B_s^0 \rightarrow D_s^{*-} \pi^+$ yield is a free parameter of the fit. The signal yield obtained from the invariant mass fit is $378\,700 \pm 700$.

The decay-time parametrisation in Eq. 1 is modified to account for the following detector effects: a decay-time-dependent reconstruction efficiency; a time-dependent decay-time resolution; the imperfect knowledge of the initial flavour of the reconstructed B_s^0 or \bar{B}_s^0 meson; the asymmetry in B_s^0 or \bar{B}_s^0 production in pp collisions; and an asymmetry in reconstruction of final state particles due to interactions in the detector material [31].

Due to the lifetime biasing effect of the selections, the reconstruction efficiency is low at small decay times and increases to a plateau after 2 ps. The decay-time-dependent reconstruction efficiency is modelled with cubic b-splines curves as described in Ref. [32]. The spline coefficients are allowed to vary in the fit to the observed decay-time distribution.

The decay-time resolution is measured using a data sample of D_s^- mesons originating from pp interactions without being required to come from an intermediate B_s^0 meson decay. These ‘prompt’ candidates pass the same real-time selection procedure as for the signal sample. After real-time selection, additional requirements are applied to ensure a D_s^- signal peak with high background rejection but without any requirement on displacement from the pp collision point. The multivariate classifier trained using the full signal decay is not applied. The reconstructed decay time in this control sample is proportional to the distance between the D_s^- production vertex and an artificial B_s^0 decay vertex, formed by combining the prompt D_s^- meson with a π^+ track from the same pp collision. It is therefore compatible with zero decay time up to bias and resolution effects. A linear relationship is observed between the decay-time resolution measured at zero decay time

and the decay-time uncertainty estimated in the vertex fit. This relationship is used to calibrate the $B_s^0 \rightarrow D_s^- \pi^+$ decay-time uncertainty. Simulated prompt D_s^- and $B_s^0 \rightarrow D_s^- \pi^+$ decays, for which the generated decay time is known, are used to check the suitability of this method, which determines a 0.005 ps bias in the reconstructed decay time due to residual detector misalignments. This bias is corrected for in the analysis. The uncertainty on Δm_s due to these residual detector misalignments, is evaluated using simulated samples that were intentionally misaligned. This uncertainty is reported in Table 1.

To determine if a neutral meson oscillated into its antiparticle, knowledge of the B_s^0 or \bar{B}_s^0 flavour at production and decay is required. In $B_s^0 \rightarrow D_s^- \pi^+$ decays, the B_s^0 flavour at decay is identified by the charge of the pion as the $D_s^+ \pi^-$ decay cannot be produced directly. To determine whether the B_s^0 oscillated before decay, the flavour at production is inferred from the hadronisation of the B_s^0 meson or the decay of other beauty hadrons produced in the collision using a combination of several flavour-tagging algorithms [33–36]. Each algorithm estimates the probability that a candidate has been assigned the wrong flavour tag. The algorithms that use information independent of signal fragmentation are calibrated using B^+ meson decays and a combined wrong-tag estimate is used in the fit. The tagging efficiency is measured to be $\varepsilon = (80.30 \pm 0.07)\%$ with a probability to tag a candidate as the wrong flavour of $\omega = (36.21 \pm 0.17)\%$, where the uncertainties account for the calibration.

In the unbinned maximum likelihood fit to the decay-time distribution used to extract Δm_s , the calibration parameters for the combined wrong tag estimate are allowed to vary. Additional free parameters are the values of the spline coefficients used to describe the decay-time-dependent reconstruction efficiency and the B_s^0 – \bar{B}_s^0 production and detection asymmetries.

The parameters Γ_s and $\Delta\Gamma_s$, are fixed in the fit to their known values [37]. Other fixed parameters are: the estimate of the wrong-tag fraction and efficiency of the tagging algorithms, the decay-time bias correction and the decay-time resolution calibration parameters. The decay-time distribution of the tagged–mixed, $\bar{B}_s^0 \rightarrow D_s^- \pi^+$, tagged–unmixed, $B_s^0 \rightarrow D_s^- \pi^+$, and untagged, where the initial flavour is unknown, samples are shown in Fig. 2 (left). The corresponding fit projection is overlaid. In order to highlight the oscillation phenomenon, the asymmetry distribution between the tagged–unmixed and tagged–mixed samples is defined as

$$A(t) = \frac{N(B_s^0 \rightarrow D_s^- \pi^+, t) - N(\bar{B}_s^0 \rightarrow D_s^- \pi^+, t)}{N(B_s^0 \rightarrow D_s^- \pi^+, t) + N(\bar{B}_s^0 \rightarrow D_s^- \pi^+, t)}, \quad (2)$$

with t modulo $2\pi/\Delta m_s$, and is shown in Fig. 2 (right). Here, $N(\bar{B}_s^0 \rightarrow D_s^- \pi^+, t)$ and $N(B_s^0 \rightarrow D_s^- \pi^+, t)$ indicate respectively the tagged–mixed and tagged–unmixed decays observed at a time t . For this distribution each event, in addition to the weight used to statistically subtract the background, is also weighted by the product of two factors. The first is a flavour-tagging dilution factor, related to the probability that the flavour tag is indeed correct. The second is an effective decay-time uncertainty dilution factor, depending on the reconstructed decay time per-event resolution and on Δm_s , for which the central value of the decay time fit is being used. The continuous line overlaid corresponds to the fit result. The result of the fit for Δm_s is $17.7683 \pm 0.0051 \text{ ps}^{-1}$, where this uncertainty is related to the sample size.

Several sources of systematic uncertainty have been investigated and those with a non-negligible contribution are listed in Table 1. These include the uncertainty on the

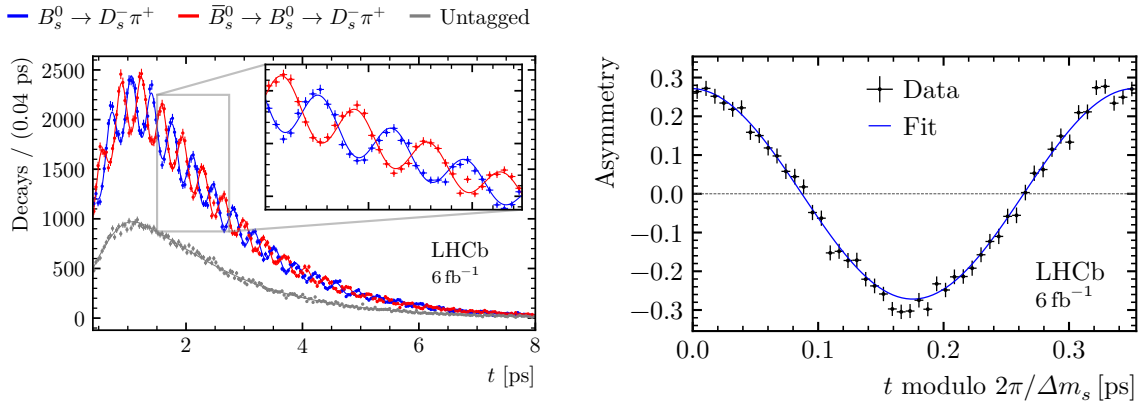


Figure 2: **Decay-time distribution of the signal decays.** Distribution of the (left) decay time of the $B_s^0 \rightarrow D_s^- \pi^+$ signal decays and (right) decay-time asymmetry between mixed and unmixed signal decays. The vertical bars correspond to the statistical uncertainty on the number of observed candidates in each bin. The horizontal bars represent the bin width. In the left plot, the horizontal bin width is indicated on the vertical axis legend. The three components, unmixed, mixed and untagged, are shown in blue, red and gray, respectively. The insert corresponds to a zoom of the region delineated in gray. The fit described in the text is overlaid.

momentum scale of the detector, obtained by comparing the reconstructed masses of known particles with the most accurate available values [37]; residual detector misalignment and length scale uncertainties; and uncertainties due to the choice of mass and decay-time fit models, determined using alternate parametrisations and pseudoexperiments. To verify the robustness of the measurement to variations in Δm_s as a function of the decay kinematics, the data sample is split into mutually disjoint subsamples, each having the same statistical significance, in relevant kinematic quantities, such as the B_s^0 momentum, and the Δm_s values obtained from each subsample are compared. The largest observed variation is included as a systematic uncertainty. The total systematic uncertainty is 0.0032 ps^{-1} , with the leading contribution due to residual detector misalignment and detector length scale uncertainties.

The value of the B_s^0 – \bar{B}_s^0 oscillation frequency determined in this article:

$$\Delta m_s = 17.7683 \pm 0.0051 \text{ (stat)} \pm 0.0032 \text{ (syst)} \text{ ps}^{-1}$$

is the most precise measurement to date. The precision is further enhanced by combining this result with the values determined in Refs. [9, 12]. Reference [9] uses $B_s^0 \rightarrow D_s^- \pi^+$ decays collected in 2011. Reference [12] uses a sample of $B_s^0 \rightarrow D_s^- \pi^+ \pi^+ \pi^-$ decays selected from the combined 2011–2018 data set, corresponding to 9 fb^{-1} . The measurements are statistically independent. The systematic uncertainties related to the momentum scale, length scale and residual detector misalignment are assumed to be fully correlated. Due to aging of the detector and different alignment procedures used in Run 1 and Run 2, the effect of residual detector misalignment is larger in measurements using Run 2 data. Given the precision of the measurement described in this paper, a detailed study of the detector misalignment effects is performed and the related uncertainty due to the decay time bias has been reduced significantly compared to previous measurements using the Run 2 data. The values of the fixed parameters $\Delta \Gamma_s$ and Γ_s used as inputs to the previous analyses have evolved over time as additional measurements have been made. However as

Table 1: **Systematic uncertainties affecting the measurement of Δm_s .** Sources of systematic uncertainties are discussed in the text. Additional details are provided in the Methods section. The total systematic uncertainty is obtained by adding the contributions in quadrature.

Description	Systematic uncertainty [ps ⁻¹]
Reconstruction effects:	
momentum scale uncertainty	0.0007
detector length scale	0.0018
detector misalignment	0.0020
Invariant mass fit model:	
background parametrisation	0.0002
$B_s^0 \rightarrow D_s^{*-} \pi^+$ and $B^0 \rightarrow D_s^- \pi^+$ contributions	0.0005
Decay-time fit model:	
decay-time resolution model	0.0011
neglecting correlation among observables	0.0011
Cross-checks:	
kinematic correlations	0.0003
Total systematic uncertainty	0.0032

the correlation between Δm_s and $\Delta \Gamma_s$ and Γ_s is negligible these small differences have been ignored in the combination procedure. A covariance matrix is constructed by adding statistical and systematic uncertainties in quadrature for each input, including correlations between systematic uncertainties. The results are averaged by minimizing the χ^2 from the full covariance matrix. The value of Δm_s obtained is $17.7666 \pm 0.0057 \text{ ps}^{-1}$. Additionally, these results are combined with those from Refs. [10, 11] where Δm_s is determined using $B_s^0 \rightarrow J/\psi K^+ K^-$ decays in the 2011–2012 (3 fb^{-1}) and 2015–2016 (2 fb^{-1}) data sets, respectively. The decay-time resolution for the measurements used in the combination, see Refs. [9–12], including the analysis presented here, varies from 35 to 45 fs, depending on the decay mode. The result for Δm_s is $17.7656 \pm 0.0057 \text{ ps}^{-1}$. The different measurements, and the resulting combination, are shown in Fig. 3.

In summary, this paper presents the most precise measurement of the Δm_s oscillation frequency, $17.7683 \pm 0.0051 \text{ (stat)} \pm 0.0032 \text{ (syst)} \text{ ps}^{-1}$, where the first uncertainty is statistical and the second systematic. The result is obtained using a sample of $B_s^0 \rightarrow D_s^- \pi^+$ decays collected with the LHCb detector during Run 2 of the LHC. Combining the result of this paper with previous measurements by the LHCb collaboration yields a Δm_s value of $17.7656 \pm 0.0057 \text{ ps}^{-1}$. This value is compatible with, and considerably more precise than, the predicted value from lattice QCD [13–15] and sum rule calculations [16, 17] of $18.4_{-1.2}^{+0.7} \text{ ps}^{-1}$ [18]. The combined result represents a significant improvement over previous measurements, and is a legacy measurement of the original LHCb detector. The experiment is currently undergoing a major upgrade to operate at five times the instantaneous luminosity from 2022 onwards [38]. The largest sources of systematic uncertainty for this measurement, namely those related to the detector length scale and misalignment, will be a focal point to further improve upon this result for future data taking periods.

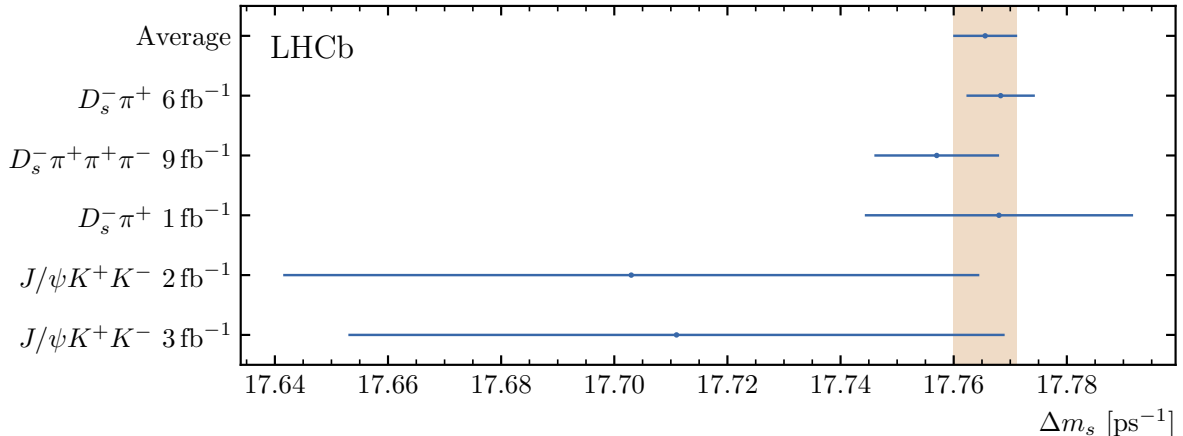


Figure 3: **Summary of LHCb measurements.** Comparison of LHCb Δm_s measurements from Refs. [9–12], the result presented in this article and their average. The measurement described in this paper is labeled as $D_s^- \pi^+$ 6 fb⁻¹. The horizontal bars correspond to the total uncertainty reported for each measurement. The band indicates the size of the uncertainty on the average for comparison purposes. The combination procedure and inputs are described in the text.

Methods

The LHCb detector. The LHCb detector [19, 20] is a single-arm forward spectrometer covering the pseudorapidity range $2 < \eta < 5$, designed for the study of particles containing b or c quarks. The detector includes a high-precision tracking system consisting of a silicon-strip vertex detector surrounding the pp interaction region [39], a large-area silicon-strip detector located upstream of a dipole magnet with a bending power of about 4 Tm, and three stations of silicon-strip detectors and straw drift tubes [40] placed downstream of the magnet. The tracking system provides a measurement of the momentum, p , of charged particles with a relative uncertainty that varies from 0.5% at low momentum to 1.0% at 200 GeV/ c . The minimum distance of a track to a primary vertex (PV), the impact parameter (IP), is measured with a resolution of $(15 + 29/p_T) \mu\text{m}$, where p_T is the component of the momentum transverse to the beam, in GeV/ c . Different types of charged hadrons are distinguished using information from two ring-imaging Cherenkov detectors [41]. Photons, electrons and hadrons are identified by a calorimeter system consisting of scintillating-pad and preshower detectors, an electromagnetic and a hadronic calorimeter. Muons are identified by a system composed of alternating layers of iron and multiwire proportional chambers [42].

Simulation of the LHCb detector response is required to model the effects of the detector acceptance and the imposed selection requirements. In the simulation, pp collisions are generated using PYTHIA [21] with a specific LHCb configuration [22]. Decays of unstable particles are described by EVTGEN [23], in which final-state radiation is generated using PHOTOS [26]. The interaction of the generated particles with the detector, and its response, are implemented using the GEANT4 toolkit [24] as described in Ref. [25].

Selection. A fast decision about which pp collisions are of interest is made by a trigger system [43]. It consists of a hardware stage, based on information from the calorimeter and muon systems, followed by a software stage, which reconstructs the pp collision based

on all available detector information. The software trigger selects candidates consistent with a b -hadron decay topology, with tracks originating from a vertex detached from the primary pp collision point, known as the primary vertex (PV). The mean B_s^0 lifetime is 1.5 ps [37], which corresponds to an average flight distance of 1 cm in the LHCb detector.

After being accepted by the trigger, a further selection is applied which forms $D_s^- \rightarrow K^- K^+ \pi^-$ and $D_s^- \rightarrow \pi^- \pi^+ \pi^-$ candidates from reconstructed charged tracks and subsequently combines them with a fourth track to form $B_s^0 \rightarrow D_s^- \pi^+$ candidates. Particle identification information is used to assign mass hypotheses to each of the final-state tracks.

The B_s^0 invariant-mass resolution is improved by constraining the D_s^- invariant mass to its known value [37]. The $K^+ K^- \pi^\pm$ or $\pi^+ \pi^- \pi^\pm$ and $D_s^- \pi^+$ invariant-mass ranges considered in this analysis are [1930, 2015] and [5300, 5800] MeV/ c^2 , respectively.

To suppress B_s^0 candidates formed from random track combinations, a gradient boosted decision tree (BDT) is used, implemented in the XGBoost library [44]. The training uses data for both the signal and the background samples in order to avoid mismatches between data and simulation. This classifier uses information on: the fit quality of the D_s^- and B_s^0 decay vertices; the D_s^- and B_s^0 χ_{IP}^2 defined as the difference in the χ^2 of the vertex fit for a given PV reconstructed with and without the considered particle; the angles between their momentum vector and the vector connecting their production and decay vertices; and the p_{T} and impact parameter χ_{IP}^2 of the final-state tracks. The BDT classifier threshold is chosen to maximize the product of the signal significance and the signal efficiency. This choice optimises sensitivity to the oscillation frequency.

Flavour tagging. The initial flavour of the B_s^0 meson must be known in order to determine if it has oscillated prior to decay. Flavour tagging algorithms are used to determine the initial flavour from properties of the b -hadron production in the pp collision.

Beauty quarks are predominantly produced in pairs. Opposite side (OS) tagging algorithms [34] determine the initial flavour of the B_s^0 meson based on information from the other beauty-quark decay. These include the OS muon and OS electron taggers, which identify the flavour from the charge of leptons produced in the other b -hadron decay. The OS kaon tagger identifies $b \rightarrow c \rightarrow s$ transitions, the OS charm quark tagger identifies $b \rightarrow c$ transitions, and the OS vertex charge tagger calculates the effective charge of an OS displaced vertex [35]. In addition, a same side (SS) kaon tagger exploits the charge information of the kaon originating from the \bar{s} or s quark leftover from the B_s^0 or \bar{B}_s^0 meson fragmentation [36]. Each algorithm determines the initial flavour of the B_s^0 meson from the charge of the reconstructed tagging particle or the reconstructed vertex in the case of the OS vertex tagger.

The tagging information is incorporated in the decay-time description. The amplitude of the oscillation is reduced by a dilution factor $D = (1 - 2\omega)$, with ω the average fraction of incorrect tags known as the mistag rate in the literature. Different machine learning algorithms provide an estimate of the mistag rate which is calibrated with data to match the true mistag distribution. A linear calibration of the average mistag as a function of the predicted mistag for the combined OS tag and SS kaon tag information is then implemented in the decay-time fit with freely varying calibration parameters. The combined tagging efficiency of the sample is $\varepsilon = (80.30 \pm 0.07)\%$ with a mistag fraction of $\omega = (36.21 \pm 0.02 \pm 0.17)\%$ where the first uncertainty is due to the finite size of the calibration sample and the second is due to the calibration procedure. This results in a combined effective performance of $(6.10 \pm 0.02 \pm 0.15)\%$ with respect to a perfect tagging

algorithm which would have a 100% tagging efficiency and zero mistag rate.

Decay time fit. The observed decay-time distribution is fitted using an unbinned maximum likelihood fit in which all combinations of initial state flavours (B_s^0 , \bar{B}_s^0 , or untagged) and final state charges ($D_s^- \pi^+$ or $D_s^+ \pi^-$) are fit simultaneously. The decay-time distribution of each measured final state is described by the sum of all processes contributing to that state. Experimental effects are taken into account with several adjustments to the theoretical prediction in eq. 1, namely:

$$P_{\text{exp.}}(B_s^0 \rightarrow D_s^- \pi^+, t) \sim (1 + a_{\text{det}}) \cdot [(1 - \omega)(1 - a_{\text{prod}})P(B_s^0 \rightarrow D_s^- \pi^+, t) + \omega(1 + a_{\text{prod}})P(\bar{B}_s^0 \rightarrow D_s^- \pi^+, t)] . \quad (3)$$

Production and detection asymmetries are parameterised by factors a_{prod} and a_{det} , respectively, which are allowed to deviate from unity. The decay-time distribution of both flavours contain a fraction $1 - \omega$ of the correctly tagged decay-time parametrisation plus a fraction ω of the incorrectly tagged decay-time parametrisation. The mistag rate ω is obtained from a per-event estimation, after a linear calibration. Different calibration parameters are used for the B_s^0 and \bar{B}_s^0 initial flavours.

The experimental decay-time distributions of both flavours are convolved with a Gaussian function to account for the finite detector resolution. The mean of this function is shifted by the decay-time bias correction factor, and the width is obtained from a per-event estimate of the decay-time uncertainty after a linear calibration.

A decay-time dependent efficiency is finally modelled by a time dependent cubic spline function, which multiplies the decay-time distribution obtained from the previous step.

Systematic uncertainties. The following sources of systematic uncertainty have been found to give a non negligible contribution to the Δm_s measurement. These are summarised in Table 1.

The measured decay-time is inversely proportional to the B_s^0 momentum, and therefore depends upon an accurate determination of the momentum scale uncertainty of the tracking system. The uncertainty is determined by varying the B_s^0 meson momentum by $\pm 0.03\%$ (coming from a comparison of masses of different particles with their known values) in simulated signal samples. The corresponding uncertainty on Δm_s is 0.0007 ps^{-1} .

The measured decay time is also proportional to the distance the B_s^0 meson travels between production and decay, which is affected by precise knowledge of the position of the vertex detector elements along the proton beam axis. The measured uncertainty is $100 \mu\text{m}$ over a length of 1 m [39]. The corresponding uncertainty on Δm_s is 0.0018 ps^{-1} .

The relative alignment of the tracking detector elements are a source of bias in the decay-time and contribute to resolution effects. The uncertainty on Δm_s due to imprecise knowledge of this alignment has been obtained from the analysis of simulated signal samples in which the detector elements have been deliberately misaligned. Different misalignments, translations, rotations and combinations of both, have been investigated. The leading effect is due to translation along the x -axis, the axis perpendicular to the beam direction pointing towards the center of the LHC ring. As a consequence simulated signal samples have been misaligned with x -axis translations in the range between 0 and $9 \mu\text{m}$ as determined from survey results. Each misaligned simulated sample is then corrected for decay time bias in the same manner as for data, and the extracted Δm_s value is compared with the value obtained in simulation without any misalignment. This

comparison produces a corresponding uncertainty on the bias correction procedure of 0.0020 ps^{-1} .

Alternative parametrisations of the background contributions to the invariant mass fit have been obtained by using different weighting methods; the difference between these parametrisations corresponds to an uncertainty of 0.0002 ps^{-1} .

For the specific $B_s^0 \rightarrow D_s^{*-} \pi^+$ and $B^0 \rightarrow D_s^- \pi^+$ background contributions, the relative fraction of these components cannot be reliably determined from the data. Their relative contributions are nominally set to an equal mixture and varied between 0 (pure $B^0 \rightarrow D_s^- \pi^+$) and 1 (pure $B_s^0 \rightarrow D_s^{*-} \pi^+$) to determine the maximum deviation in Δm_s corresponding to an uncertainty of 0.0005 ps^{-1} .

The decay-time resolution is obtained from data using a sample of D_s^- mesons that are produced directly in pp collision. These are combined with a π^+ meson coming from the same collision to produce a fake B_s^0 candidate with a decay time equal to zero, ignoring resolution effects. Different parametrisations of the measured decay-time distribution are applied to a simulated signal sample. The largest deviation of the extracted Δm_s value with respect to the nominal parametrisation is found to be 0.0011 ps^{-1} .

The procedure used to subtract background contributions in the fit to the decay-time distribution assumes no large correlations between the decay-time and the reconstructed B_s^0 and D_s^- invariant masses. This is studied by analysing simulated signal and background samples where any residual correlations between these observables are removed. The difference in measured value of Δm_s between the decorrelated and nominal samples is found to be 0.0011 ps^{-1} .

The data sample was split into mutually disjoint subsamples in order to study the effect of potential correlations between kinematic ranges, data taking periods, flavour-tagging categories, the BDT-based selection and the measured value of Δm_s . The measured values obtained from each subsample are compared and the largest observed variation is found to be 0.0003 ps^{-1} .

Several additional effects have been considered consisting of: possible biases introduced by the fit procedure, changes to the signal and background parametrisations, and changes in the reweighting procedure used when obtaining the invariant mass shapes of partially reconstructed backgrounds constituting less than 2 % of the signal yield. Their impact has been found to be negligible with respect to the sources listed in Table 1.

The largest sources of systematic uncertainty are found to be due to imprecise knowledge of the position and alignment of the tracking detector closest to the nominal pp collision region.

Data Availability. All figures are available from:

<https://lhcbproject.web.cern.ch/Publications/p/LHCb-PAPER-2021-005.html>

Additional material describing this analysis is available from:

<http://cds.cern.ch/record/2764338/files/>

in LHCb-PAPER-2021-005-supplementary.zip as Supplementary.pdf

Inputs to the Δm_s combination are available from HEPdata at:

<https://www.hepdata.net/record/105881>

LHCb has an open data policy described in:

<http://cdsweb.cern.ch/record/1543410>

Subject to the resources being identified, LHCb will endeavor to provide open access to

some reconstructed level data on disk at CERN.

Code Availability. The code used for the fit to the B_s^0 and D_s^- invariant mass distributions and to the B_s^0 decay time distribution is publicly available at:
<https://gitlab.cern.ch/lhcb/Urania/-/tree/master/PhysFit/B2DXFitters>

Acknowledgements

We express our gratitude to our colleagues in the CERN accelerator departments for the excellent performance of the LHC. We thank the technical and administrative staff at the LHCb institutes. We acknowledge support from CERN and from the national agencies: CAPES, CNPq, FAPERJ and FINEP (Brazil); MOST and NSFC (China); CNRS/IN2P3 (France); BMBF, DFG and MPG (Germany); INFN (Italy); NWO (Netherlands); MNiSW and NCN (Poland); MEN/IFA (Romania); MSHE (Russia); MICINN (Spain); SNSF and SER (Switzerland); NASU (Ukraine); STFC (United Kingdom); DOE NP and NSF (USA). We acknowledge the computing resources that are provided by CERN, IN2P3 (France), KIT and DESY (Germany), INFN (Italy), SURF (Netherlands), PIC (Spain), GridPP (United Kingdom), RRCKI and Yandex LLC (Russia), CSCS (Switzerland), IFIN-HH (Romania), CBPF (Brazil), PL-GRID (Poland) and NERSC (USA). We are indebted to the communities behind the multiple open-source software packages on which we depend. Individual groups or members have received support from ARC and ARDC (Australia); AvH Foundation (Germany); EPLANET, Marie Skłodowska-Curie Actions and ERC (European Union); A*MIDEX, ANR, Labex P2IO and OCEVU, and Région Auvergne-Rhône-Alpes (France); Key Research Program of Frontier Sciences of CAS, CAS PIFI, CAS CCEPP, Fundamental Research Funds for the Central Universities, and Sci. & Tech. Program of Guangzhou (China); RFBR, RSF and Yandex LLC (Russia); GVA, XuntaGal and GENCAT (Spain); the Leverhulme Trust, the Royal Society and UKRI (United Kingdom).

Author contributions

All authors have contributed to the publication, being variously involved in the design and the construction of the detectors, in writing software, in operating the detectors and acquiring data, in calibrating sub-systems and processing data and finally in analysing the processed data.

Competing interests

The authors declare no competing interests.

References

- [1] A. Lenz and U. Nierste, *Theoretical update of $B_s^0-\bar{B}_s^0$ mixing*, JHEP **06** (2007) 072.

- [2] N. Cabibbo, *Unitary symmetry and leptonic decays*, Phys. Rev. Lett. **10** (1963) 531.
- [3] M. Kobayashi and T. Maskawa, *CP-violation in the renormalizable theory of weak interaction*, Prog. Theor. Phys. **49** (1973) 652.
- [4] UTfit collaboration, M. Bona *et al.*, *The unitarity triangle fit in the standard model and hadronic parameters from lattice QCD: A reappraisal after the measurements of Δm_s and $BR(B \rightarrow \tau\nu_\tau)$* , JHEP **10** (2006) 081, arXiv:hep-ph/0606167, updated results and plots available at <http://www.utfit.org/>.
- [5] CKMfitter group, J. Charles *et al.*, *Current status of the standard model CKM fit and constraints on $\Delta F = 2$ new physics*, Phys. Rev. **D91** (2015) 073007, arXiv:1501.05013, updated results and plots available at <http://ckmfitter.in2p3.fr/>.
- [6] S. Aoki, Y. Aoki, D. Bećirević *et al.*, *FLAG Review 2019*, EPJC **80** (2020) 113.
- [7] LHCb collaboration, R. Aaij *et al.*, *Measurement of CP asymmetry in $B_s^0 \rightarrow D_s^\mp K^\pm$ decays*, JHEP **03** (2018) 059, arXiv:1712.07428.
- [8] CDF collaboration, A. Abulencia *et al.*, *Observation of $B_s^0-\bar{B}_s^0$ Oscillations*, Phys. Rev. Lett. **97** (2006) 242003, arXiv:hep-ex/0609040.
- [9] LHCb collaboration, R. Aaij *et al.*, *Precision measurement of the $B_s^0-\bar{B}_s^0$ oscillation frequency in the decay $B_s^0 \rightarrow D_s^- \pi^+$* , New J. Phys. **15** (2013) 053021, arXiv:1304.4741.
- [10] LHCb collaboration, R. Aaij *et al.*, *Precision measurement of CP violation in $B_s^0 \rightarrow J/\psi K^+ K^-$ decays*, Phys. Rev. Lett. **114** (2015) 041801, arXiv:1411.3104.
- [11] LHCb collaboration, R. Aaij *et al.*, *Updated measurement of time-dependent CP-violating observables in $B_s^0 \rightarrow J/\psi K^+ K^-$ decays*, Eur. Phys. J. **C79** (2019) 706, Erratum *ibid.* **C80** (2020) 601, arXiv:1906.08356.
- [12] LHCb collaboration, R. Aaij *et al.*, *Measurement of the CKM angle γ and $B_s^0-\bar{B}_s^0$ mixing frequency with $B_s^0 \rightarrow D_s^\mp h^\pm \pi^\pm \pi^\mp$ decays*, JHEP **03** (2021) 137, arXiv:2011.12041.
- [13] A. Bazavov *et al.*, *$B^0_{(s)}$ -mixing matrix elements from lattice QCD for the Standard Model and beyond*, PRD **93** (2016) 113016.
- [14] P. A. Boyle and others (RBC/UKQCD collaboration), *$SU(3)$ -breaking ratios for $D_{(s)}$ and $B_{(s)}$ mesons*, arXiv:1812.08791.
- [15] R. J. Dowdall *et al.*, *Neutral B-meson mixing from full lattice QCD at the physical point*, PRD **100** (2019) 094508.
- [16] A. G. Grozin, T. Thomas, and A. A. Pivovarov, *$B^0-\bar{B}^0$ mixing: matching to HQET at NNLO*, PRD **98** (2018) 054020.
- [17] D. King, A. Lenz, and T. Rauh, *B_s^0 mixing observables and V_{td}/V_{ts} from sum rules*, JHEP **05** (2019) 034.

- [18] L. Di Luzio, M. Kirk, A. Lenz, and T. Rauh, ΔM_s theory precision confronts flavour anomalies, *JHEP* **12** (2019) 009.
- [19] LHCb collaboration, A. A. Alves Jr. *et al.*, *The LHCb detector at the LHC*, *JINST* **3** (2008) S08005.
- [20] LHCb collaboration, R. Aaij *et al.*, *LHCb detector performance*, *Int. J. Mod. Phys.* **A30** (2015) 1530022, [arXiv:1412.6352](#).
- [21] T. Sjöstrand, S. Mrenna, and P. Skands, *A brief introduction to PYTHIA 8.1*, *Comput. Phys. Commun.* **178** (2008) 852, [arXiv:0710.3820](#).
- [22] I. Belyaev *et al.*, *Handling of the generation of primary events in Gauss, the LHCb simulation framework*, *J. Phys. Conf. Ser.* **331** (2011) 032047.
- [23] D. J. Lange, *The EvtGen particle decay simulation package*, *Nucl. Instrum. Meth.* **A462** (2001) 152.
- [24] Geant4 collaboration, J. Allison *et al.*, *Geant4 developments and applications*, *IEEE Trans. Nucl. Sci.* **53** (2006) 270; Geant4 collaboration, S. Agostinelli *et al.*, *Geant4: A simulation toolkit*, *Nucl. Instrum. Meth.* **A506** (2003) 250.
- [25] M. Clemencic *et al.*, *The LHCb simulation application, Gauss: Design, evolution and experience*, *J. Phys. Conf. Ser.* **331** (2011) 032023.
- [26] N. Davidson, T. Przedzinski, and Z. Was, *PHOTOS interface in C++: Technical and physics documentation*, *Comp. Phys. Comm.* **199** (2016) 86, [arXiv:1011.0937](#).
- [27] R. Aaij *et al.*, *Performance of the LHCb trigger and full real-time reconstruction in Run 2 of the LHC*, *JINST* **14** (2019) P04013, [arXiv:1812.10790](#).
- [28] M. Pivk and F. R. Le Diberder, *sPlot: A statistical tool to unfold data distributions*, *Nucl. Instrum. Meth.* **A555** (2005) 356, [arXiv:physics/0402083](#).
- [29] D. Martínez Santos and F. Dupertuis, *Mass distributions marginalized over per-event errors*, *Nucl. Instrum. Meth.* **A764** (2014) 150, [arXiv:1312.5000](#).
- [30] N. L. Johnson, *Systems of frequency curves generated by methods of translation*, *Biometrika* **36** (1949) 149.
- [31] LHCb collaboration, R. Aaij *et al.*, *Measurement of B^0 , B_s^0 , B^+ and Λ_b^0 production asymmetries in 7 and 8 TeV proton-proton collisions*, *Phys. Lett.* **B774** (2017) 139, [arXiv:1703.08464](#).
- [32] M. Karbach, G. Raven, and M. Schiller, *Decay time integrals in neutral meson mixing and their efficient evaluation*, [arXiv:1407.0748](#).
- [33] D. Fazzini, *Flavour Tagging in the LHCb experiment*, in *Proceedings, 6th Large Hadron Collider Physics Conference (LHCP 2018): Bologna, Italy, June 4-9, 2018*, **LHCP2018** 230, 2018.
- [34] LHCb collaboration, R. Aaij *et al.*, *Opposite-side flavour tagging of B mesons at the LHCb experiment*, *Eur. Phys. J.* **C72** (2012) 2022, [arXiv:1202.4979](#).

- [35] LHCb collaboration, R. Aaij *et al.*, *B flavour tagging using charm decays at the LHCb experiment*, JINST **10** (2015) P10005, [arXiv:1507.07892](#).
- [36] LHCb collaboration, R. Aaij *et al.*, *A new algorithm for identifying the flavour of B_s^0 mesons at LHCb*, JINST **11** (2016) P05010, [arXiv:1602.07252](#).
- [37] Particle Data Group, P. A. Zyla *et al.*, *Review of particle physics*, Prog. Theor. Exp. Phys. **2020** (2020) 083C01.
- [38] LHCb collaboration, *Framework TDR for the LHCb Upgrade: Technical Design Report*, CERN-LHCC-2012-007, 2012.
- [39] R. Aaij *et al.*, *Performance of the LHCb Vertex Locator*, JINST **9** (2014) P09007, [arXiv:1405.7808](#).
- [40] P. d'Argent *et al.*, *Improved performance of the LHCb Outer Tracker in LHC Run 2*, JINST **12** (2017) P11016, [arXiv:1708.00819](#).
- [41] M. Adinolfi *et al.*, *Performance of the LHCb RICH detector at the LHC*, Eur. Phys. J. **C73** (2013) 2431, [arXiv:1211.6759](#).
- [42] A. A. Alves Jr. *et al.*, *Performance of the LHCb muon system*, JINST **8** (2013) P02022, [arXiv:1211.1346](#).
- [43] R. Aaij *et al.*, *The LHCb trigger and its performance in 2011*, JINST **8** (2013) P04022, [arXiv:1211.3055](#).
- [44] T. Chen and C. Guestrin, *XGBoost: A scalable tree boosting system*, in *Proceedings of the 22nd ACM SIGKDD International Conference on Knowledge Discovery and Data Mining*, KDD '16, (New York, NY, USA), 785–794, ACM, 2016.

LHCb collaboration

R. Aaij³², C. Abellán Beteta⁵⁰, T. Ackernley⁶⁰, B. Adeva⁴⁶, M. Adinolfi⁵⁴, H. Afsharnia⁹, C.A. Aidala⁸⁶, S. Aiola²⁵, Z. Ajaltouni⁹, S. Akar⁶⁵, J. Albrecht¹⁵, F. Alessio⁴⁸, M. Alexander⁵⁹, A. Alfonso Alberio⁴⁵, Z. Aliouche⁶², G. Alkhazov³⁸, P. Alvarez Cartelle⁵⁵, S. Amato², Y. Amhis¹¹, L. An⁴⁸, L. Anderlini²², A. Andreianov³⁸, M. Andreotti²¹, F. Archilli¹⁷, A. Artamonov⁴⁴, M. Artuso⁶⁸, K. Arzymatov⁴², E. Aslanides¹⁰, M. Atzeni⁵⁰, B. Audurier¹², S. Bachmann¹⁷, M. Bachmayer⁴⁹, J.J. Back⁵⁶, P. Baladron Rodriguez⁴⁶, V. Balagura¹², W. Baldini²¹, J. Baptista Leite¹, R.J. Barlow⁶², S. Barsuk¹¹, W. Barter⁶¹, M. Bartolini²⁴, F. Baryshnikov⁸³, J.M. Basels¹⁴, G. Bassi²⁹, B. Batsukh⁶⁸, A. Battig¹⁵, A. Bay⁴⁹, M. Becker¹⁵, F. Bedeschi²⁹, I. Bediaga¹, A. Beiter⁶⁸, V. Belavin⁴², S. Belin²⁷, V. Bellee⁴⁹, K. Belous⁴⁴, I. Belov⁴⁰, I. Belyaev⁴¹, G. Bencivenni²³, E. Ben-Haim¹³, A. Berezhnoy⁴⁰, R. Bernet⁵⁰, D. Berninghoff¹⁷, H.C. Bernstein⁶⁸, C. Bertella⁴⁸, A. Bertolin²⁸, C. Betancourt⁵⁰, F. Betti⁴⁸, Ia. Bezshyiko⁵⁰, S. Bhasin⁵⁴, J. Bhom³⁵, L. Bian⁷³, M.S. Bieker¹⁵, S. Bifani⁵³, P. Billoir¹³, M. Birch⁶¹, F.C.R. Bishop⁵⁵, A. Bitadze⁶², A. Bizzeti^{22,k}, M. Bjørn⁶³, M.P. Blago⁴⁸, T. Blake⁵⁶, F. Blanc⁴⁹, S. Blusk⁶⁸, D. Bobulska⁵⁹, J.A. Boelhauve¹⁵, O. Boente Garcia⁴⁶, T. Boettcher⁶⁴, A. Boldyrev⁸², A. Bondar⁴³, N. Bondar^{38,48}, S. Borghi⁶², M. Borisyak⁴², M. Borsato¹⁷, J.T. Borsuk³⁵, S.A. Bouchiba⁴⁹, T.J.V. Bowcock⁶⁰, A. Boyer⁴⁸, C. Bozzi²¹, M.J. Bradley⁶¹, S. Braun⁶⁶, A. Brea Rodriguez⁴⁶, M. Brodski⁴⁸, J. Brodzicka³⁵, A. Brossa Gonzalo⁵⁶, D. Brundu²⁷, A. Buonauro⁵⁰, C. Burr⁴⁸, A. Bursche⁷², A. Butkevich³⁹, J.S. Butter³², J. Buytaert⁴⁸, W. Byczynski⁴⁸, S. Cadeddu²⁷, H. Cai⁷³, R. Calabrese^{21,f}, L. Calefice^{15,13}, L. Calero Diaz²³, S. Cali²³, R. Calladine⁵³, M. Calvi^{26,j}, M. Calvo Gomez⁸⁵, P. Camargo Magalhaes⁵⁴, A. Camboni^{45,85}, P. Campana²³, A.F. Campoverde Quezada⁶, S. Capelli^{26,j}, L. Capriotti^{20,d}, A. Carbone^{20,d}, G. Carboni³¹, R. Cardinale²⁴, A. Cardini²⁷, I. Carli⁴, P. Carniti^{26,j}, L. Carus¹⁴, K. Carvalho Akiba³², A. Casais Vidal⁴⁶, G. Casse⁶⁰, M. Cattaneo⁴⁸, G. Cavallero⁴⁸, S. Celani⁴⁹, J. Cerasoli¹⁰, A.J. Chadwick⁶⁰, M.G. Chapman⁵⁴, M. Charles¹³, Ph. Charpentier⁴⁸, G. Chatzikonstantinidis⁵³, C.A. Chavez Barajas⁶⁰, M. Chefdeville⁸, C. Chen³, S. Chen⁴, A. Chernov³⁵, V. Chobanova⁴⁶, S. Cholak⁴⁹, M. Chruszcz³⁵, A. Chubykin³⁸, V. Chulikov³⁸, P. Ciambone²³, M.F. Cicala⁵⁶, X. Cid Vidal⁴⁶, G. Ciezarek⁴⁸, P.E.L. Clarke⁵⁸, M. Clemencic⁴⁸, H.V. Cliff⁵⁵, J. Closier⁴⁸, J.L. Cobbedick⁶², V. Coco⁴⁸, J.A.B. Coelho¹¹, J. Cogan¹⁰, E. Cogneras⁹, L. Cojocariu³⁷, P. Collins⁴⁸, T. Colombo⁴⁸, L. Congedo^{19,c}, A. Contu²⁷, N. Cooke⁵³, G. Coombs⁵⁹, G. Corti⁴⁸, C.M. Costa Sobral⁵⁶, B. Couturier⁴⁸, D.C. Craik⁶⁴, J. Crkovačka⁶⁷, M. Cruz Torres¹, R. Currie⁵⁸, C.L. Da Silva⁶⁷, E. Dall'Occo¹⁵, J. Dalseno⁴⁶, C. D'Ambrosio⁴⁸, A. Danilina⁴¹, P. d'Argent⁴⁸, A. Davis⁶², O. De Aguiar Francisco⁶², K. De Bruyn⁷⁹, S. De Capua⁶², M. De Cian⁴⁹, J.M. De Miranda¹, L. De Paula², M. De Serio^{19,c}, D. De Simone⁵⁰, P. De Simone²³, J.A. de Vries⁸⁰, C.T. Dean⁶⁷, D. Decamp⁸, L. Del Buono¹³, B. Delaney⁵⁵, H.-P. Dembinski¹⁵, A. Dendek³⁴, V. Denysenko⁵⁰, D. Derkach⁸², O. Deschamps⁹, F. Desse¹¹, F. Dettori^{27,e}, B. Dey⁷⁷, P. Di Nezza²³, S. Didenko⁸³, L. Dieste Maronas⁴⁶, H. Dijkstra⁴⁸, V. Dobishuk⁵², A.M. Donohoe¹⁸, F. Dordei²⁷, A.C. dos Reis¹, L. Douglas⁵⁹, A. Dovbnya⁵¹, A.G. Downes⁸, K. Dreimanis⁶⁰, M.W. Dudek³⁵, L. Dufour⁴⁸, V. Duk⁷⁸, P. Durante⁴⁸, J.M. Durham⁶⁷, D. Dutta⁶², A. Dziurda³⁵, A. Dzyuba³⁸, S. Easo⁵⁷, U. Egede⁶⁹, V. Egorychev⁴¹, S. Eidelman^{43,v}, S. Eisenhardt⁵⁸, S. Ek-In⁴⁹, L. Eklund^{59,w}, S. Ely⁶⁸, A. Ene³⁷, E. Epple⁶⁷, S. Escher¹⁴, J. Eschle⁵⁰, S. Esen¹³, T. Evans⁴⁸, A. Falabella²⁰, J. Fan³, Y. Fan⁶, B. Fang⁷³, S. Farry⁶⁰, D. Fazzini^{26,j}, M. Féo⁴⁸, A. Fernandez Prieto⁴⁶, J.M. Fernandez-tenllado Arribas⁴⁵, A.D. Fernez⁶⁶, F. Ferrari^{20,d}, L. Ferreira Lopes⁴⁹, F. Ferreira Rodrigues², S. Ferreres Sole³², M. Ferrillo⁵⁰, M. Ferro-Luzzi⁴⁸, S. Filippov³⁹, R.A. Fini¹⁹, M. Fiorini^{21,f}, M. Firlej³⁴, K.M. Fischer⁶³, D.S. Fitzgerald⁸⁶, C. Fitzpatrick⁶², T. Fiutowski³⁴, F. Fleuret¹², M. Fontana¹³, F. Fontanelli^{24,h}, R. Forty⁴⁸, V. Franco Lima⁶⁰, M. Franco Sevilla⁶⁶, M. Frank⁴⁸, E. Franzoso²¹, G. Frau¹⁷, C. Frei⁴⁸, D.A. Friday⁵⁹, J. Fu²⁵, Q. Fuehring¹⁵, W. Funk⁴⁸, E. Gabriel³²,

T. Gaintseva⁴², A. Gallas Torreira⁴⁶, D. Galli^{20,d}, S. Gambetta^{58,48}, Y. Gan³, M. Gandelman²,
 P. Gandini²⁵, Y. Gao⁵, M. Garau²⁷, L.M. Garcia Martin⁵⁶, P. Garcia Moreno⁴⁵,
 J. García Pardiñas^{26,j}, B. Garcia Plana⁴⁶, F.A. Garcia Rosales¹², L. Garrido⁴⁵, C. Gaspar⁴⁸,
 R.E. Geertsema³², D. Gerick¹⁷, L.L. Gerken¹⁵, E. Gersabeck⁶², M. Gersabeck⁶², T. Gershon⁵⁶,
 D. Gerstel¹⁰, Ph. Ghez⁸, V. Gibson⁵⁵, H.K. Giezma³⁶, M. Giovannetti^{23,p}, A. Gioventù⁴⁶,
 P. Gironella Gironell⁴⁵, L. Giubega³⁷, C. Giugliano^{21,f,48}, K. Gizdov⁵⁸, E.L. Gkougkousis⁴⁸,
 V.V. Gligorov¹³, C. Göbel⁷⁰, E. Golobardes⁸⁵, D. Golubkov⁴¹, A. Golutvin^{61,83}, A. Gomes^{1,a},
 S. Gomez Fernandez⁴⁵, F. Goncalves Abrantes⁶³, M. Goncerz³⁵, G. Gong³, P. Gorbounov⁴¹,
 I.V. Gorelov⁴⁰, C. Gotti²⁶, E. Govorkova⁴⁸, J.P. Grabowski¹⁷, T. Grammatico¹³,
 L.A. Granado Cardoso⁴⁸, E. Graugés⁴⁵, E. Graverini⁴⁹, G. Graziani²², A. Grecu³⁷,
 L.M. Greeven³², P. Griffith^{21,f}, L. Grillo⁶², S. Gromov⁸³, B.R. Gruberg Cazon⁶³, C. Gu³,
 M. Guarise²¹, P. A. Günther¹⁷, E. Gushchin³⁹, A. Guth¹⁴, Y. Guz⁴⁴, T. Gys⁴⁸,
 T. Hadavizadeh⁶⁹, G. Haefeli⁴⁹, C. Haen⁴⁸, J. Haimberger⁴⁸, T. Halewood-leagas⁶⁰,
 P.M. Hamilton⁶⁶, J.P. Hammerich⁶⁰, Q. Han⁷, X. Han¹⁷, T.H. Hancock⁶³,
 S. Hansmann-Menzemer¹⁷, N. Harnew⁶³, T. Harrison⁶⁰, C. Hasse⁴⁸, M. Hatch⁴⁸, J. He^{6,b},
 M. Hecker⁶¹, K. Heijhoff³², K. Heinicke¹⁵, A.M. Hennequin⁴⁸, K. Hennessy⁶⁰, L. Henry^{25,47},
 J. Heuel¹⁴, A. Hicheur², D. Hill⁴⁹, M. Hilton⁶², S.E. Hollitt¹⁵, J. Hu¹⁷, J. Hu⁷², W. Hu⁷,
 W. Huang⁶, X. Huang⁷³, W. Hulsbergen³², R.J. Hunter⁵⁶, M. Hushchyn⁸², D. Hutchcroft⁶⁰,
 D. Hynds³², P. Ibis¹⁵, M. Idzik³⁴, D. Ilin³⁸, P. Ilten⁶⁵, A. Inglese³⁸, A. Ishteev⁸³, K. Ivshin³⁸,
 R. Jacobsson⁴⁸, S. Jakobsen⁴⁸, E. Jans³², B.K. Jashal⁴⁷, A. Jawahery⁶⁶, V. Jevtic¹⁵,
 M. Jezabek³⁵, F. Jiang³, M. John⁶³, D. Johnson⁴⁸, C.R. Jones⁵⁵, T.P. Jones⁵⁶, B. Jost⁴⁸,
 N. Jurik⁴⁸, S. Kandybei⁵¹, Y. Kang³, M. Karacson⁴⁸, M. Karpov⁸², F. Keizer⁴⁸, M. Kenzie⁵⁶,
 T. Ketel³³, B. Khanji¹⁵, A. Kharisova⁸⁴, S. Kholodenko⁴⁴, T. Kirn¹⁴, V.S. Kirsebom⁴⁹,
 O. Kitouni⁶⁴, S. Klaver³², K. Klimaszewski³⁶, S. Koliiev⁵², A. Kondybayeva⁸³,
 A. Konoplyannikov⁴¹, P. Kopciwicz³⁴, R. Kopecna¹⁷, P. Koppenburg³², M. Korolev⁴⁰,
 I. Kostiuik^{32,52}, O. Kot⁵², S. Kotriakhova^{21,38}, P. Kravchenko³⁸, L. Kravchuk³⁹,
 R.D. Krawczyk⁴⁸, M. Kreps⁵⁶, F. Kress⁶¹, S. Kretzschmar¹⁴, P. Krokovny^{43,v}, W. Krupa³⁴,
 W. Krzemien³⁶, W. Kucewicz^{35,t}, M. Kucharczyk³⁵, V. Kudryavtsev^{43,v}, H.S. Kuindersma^{32,33},
 G.J. Kunde⁶⁷, T. Kvaratskheliya⁴¹, D. Lacarrere⁴⁸, G. Lafferty⁶², A. Lai²⁷, A. Lampis²⁷,
 D. Lancierini⁵⁰, J.J. Lane⁶², R. Lane⁵⁴, G. Lanfranchi²³, C. Langenbruch¹⁴, J. Langer¹⁵,
 O. Lantwin⁵⁰, T. Latham⁵⁶, F. Lazzari^{29,q}, R. Le Gac¹⁰, S.H. Lee⁸⁶, R. Lefèvre⁹, A. Leflat⁴⁰,
 S. Legotin⁸³, O. Leroy¹⁰, T. Lesiak³⁵, B. Leverington¹⁷, H. Li⁷², L. Li⁶³, P. Li¹⁷, S. Li⁷, Y. Li⁴,
 Y. Li⁴, Z. Li⁶⁸, X. Liang⁶⁸, T. Lin⁶¹, R. Lindner⁴⁸, V. Lisovskyi¹⁵, R. Litvinov²⁷, G. Liu⁷²,
 H. Liu⁶, S. Liu⁴, X. Liu³, A. Loi²⁷, J. Lomba Castro⁴⁶, I. Longstaff⁵⁹, J.H. Lopes²,
 G.H. Lovell⁵⁵, Y. Lu⁴, D. Lucchesi^{28,l}, S. Luchuk³⁹, M. Lucio Martinez³², V. Lukashenko³²,
 Y. Luo³, A. Lupato⁶², E. Luppi^{21,f}, O. Lupton⁵⁶, A. Lusiani^{29,m}, X. Lyu⁶, L. Ma⁴, R. Ma⁶,
 S. Maccolini^{20,d}, F. Machefert¹¹, F. Maciuc³⁷, V. Macko⁴⁹, P. Mackowiak¹⁵,
 S. Maddrell-Mander⁵⁴, O. Madejczyk³⁴, L.R. Madhan Mohan⁵⁴, O. Maev³⁸, A. Maevskiy⁸²,
 D. Maisuzenko³⁸, M.W. Majewski³⁴, J.J. Malczewski³⁵, S. Malde⁶³, B. Malecki⁴⁸, A. Malinin⁸¹,
 T. Maltsev^{43,v}, H. Malygina¹⁷, G. Manca^{27,e}, G. Mancinelli¹⁰, D. Manuzzi^{20,d},
 D. Marangotto^{25,i}, J. Maratas^{9,s}, J.F. Marchand⁸, U. Marconi²⁰, S. Mariani^{22,g},
 C. Marin Benito⁴⁸, M. Marinangeli⁴⁹, J. Marks¹⁷, A.M. Marshall⁵⁴, P.J. Marshall⁶⁰,
 G. Martellotti³⁰, L. Martinazzoli^{48,j}, M. Martinelli^{26,j}, D. Martinez Santos⁴⁶,
 F. Martinez Vidal⁴⁷, A. Massafferri¹, M. Materok¹⁴, R. Matev⁴⁸, A. Mathad⁵⁰, Z. Mathe⁴⁸,
 V. Matiunin⁴¹, C. Matteuzzi²⁶, K.R. Mattioli⁸⁶, A. Mauri³², E. Maurice¹², J. Mauricio⁴⁵,
 M. Mazurek⁴⁸, M. McCann⁶¹, L. Mcconnell¹⁸, T.H. Mcgrath⁶², A. McNab⁶², R. McNulty¹⁸,
 J.V. Mead⁶⁰, B. Meadows⁶⁵, C. Meaux¹⁰, G. Meier¹⁵, N. Meinert⁷⁶, D. Melnychuk³⁶,
 S. Meloni^{26,j}, M. Merk^{32,80}, A. Merli²⁵, L. Meyer Garcia², M. Mikhasenko⁴⁸, D.A. Milanese⁷⁴,
 E. Millard⁵⁶, M. Milovanovic⁴⁸, M.-N. Minard⁸, A. Minotti²¹, L. Minzoni^{21,f}, S.E. Mitchell⁵⁸,
 B. Mitreska⁶², D.S. Mitzel⁴⁸, A. Mödden¹⁵, R.A. Mohammed⁶³, R.D. Moise⁶¹, T. Mombächer¹⁵,

I.A. Monroy⁷⁴, S. Monteil⁹, M. Morandin²⁸, G. Morello²³, M.J. Morello^{29,m}, J. Moron³⁴,
 A.B. Morris⁷⁵, A.G. Morris⁵⁶, R. Mountain⁶⁸, H. Mu³, F. Muheim^{58,48}, M. Mulder⁴⁸,
 D. Müller⁴⁸, K. Müller⁵⁰, C.H. Murphy⁶³, D. Murray⁶², P. Muzzetto^{27,48}, P. Naik⁵⁴,
 T. Nakada⁴⁹, R. Nandakumar⁵⁷, T. Nanut⁴⁹, I. Nasteva², M. Needham⁵⁸, I. Neri²¹, N. Neri^{25,i},
 S. Neubert⁷⁵, N. Neufeld⁴⁸, R. Newcombe⁶¹, T.D. Nguyen⁴⁹, C. Nguyen-Mau^{49,x}, E.M. Niel¹¹,
 S. Nieswand¹⁴, N. Nikitin⁴⁰, N.S. Nolte¹⁵, C. Nunez⁸⁶, A. Oblakowska-Mucha³⁴, V. Obraztsov⁴⁴,
 D.P. O'Hanlon⁵⁴, R. Oldeman^{27,e}, M.E. Olivares⁶⁸, C.J.G. Onderwater⁷⁹, A. Ossowska³⁵,
 J.M. Otalora Goicochea², T. Ovsianikova⁴¹, P. Owen⁵⁰, A. Oyanguren⁴⁷, B. Pagare⁵⁶,
 P.R. Pais⁴⁸, T. Pajero⁶³, A. Palano¹⁹, M. Palutan²³, Y. Pan⁶², G. Panshin⁸⁴, A. Papanestis⁵⁷,
 M. Pappagallo^{19,c}, L.L. Pappalardo^{21,f}, C. Pappenheimer⁶⁵, W. Parker⁶⁶, C. Parkes⁶²,
 C.J. Parkinson⁴⁶, B. Passalacqua²¹, G. Passaleva²², A. Pastore¹⁹, M. Patel⁶¹, C. Patrignani^{20,d},
 C.J. Pawley⁸⁰, A. Pearce⁴⁸, A. Pellegrino³², M. Pepe Altarelli⁴⁸, S. Perazzini²⁰, D. Pereima⁴¹,
 P. Perret⁹, M. Petric^{59,48}, K. Petridis⁵⁴, A. Petrolini^{24,h}, A. Petrov⁸¹, S. Petrucci⁵⁸,
 M. Petruzzo²⁵, T.T.H. Pham⁶⁸, A. Philippov⁴², L. Pica^{29,n}, M. Piccini⁷⁸, B. Pietrzyk⁸,
 G. Pietrzyk⁴⁹, M. Pili⁶³, D. Pinci³⁰, F. Pisani⁴⁸, Resmi P.K¹⁰, V. Placinta³⁷, J. Plews⁵³,
 M. Plo Casasus⁴⁶, F. Polci¹³, M. Poli Lener²³, M. Poliakov⁶⁸, A. Poluektov¹⁰, N. Polukhina^{83,u},
 I. Polyakov⁶⁸, E. Polycarpo², G.J. Pomery⁵⁴, S. Ponce⁴⁸, D. Popov^{6,48}, S. Popov⁴²,
 S. Poslavskii⁴⁴, K. Prasanth³⁵, L. Promberger⁴⁸, C. Prouve⁴⁶, V. Pugatch⁵², H. Pullen⁶³,
 G. Punzi^{29,n}, W. Qian⁶, J. Qin⁶, R. Quagliani¹³, B. Quintana⁸, N.V. Raab¹⁸,
 R.I. Rabadan Trejo¹⁰, B. Rachwal³⁴, J.H. Rademacker⁵⁴, M. Rama²⁹, M. Ramos Pernas⁵⁶,
 M.S. Rangel², F. Ratnikov^{42,82}, G. Raven³³, M. Reboud⁸, F. Redi⁴⁹, F. Reiss⁶²,
 C. Remon Alepuz⁴⁷, Z. Ren³, V. Renaudin⁶³, R. Ribatti²⁹, S. Ricciardi⁵⁷, K. Rinnert⁶⁰,
 P. Robbe¹¹, G. Robertson⁵⁸, A.B. Rodrigues⁴⁹, E. Rodrigues⁶⁰, J.A. Rodriguez Lopez⁷⁴,
 A. Rollings⁶³, P. Roloff⁴⁸, V. Romanovskiy⁴⁴, M. Romero Lamas⁴⁶, A. Romero Vidal⁴⁶,
 J.D. Roth⁸⁶, M. Rotondo²³, M.S. Rudolph⁶⁸, T. Ruf⁴⁸, J. Ruiz Vidal⁴⁷, A. Ryzhikov⁸²,
 J. Ryzka³⁴, J.J. Saborido Silva⁴⁶, N. Sagidova³⁸, N. Sahoo⁵⁶, B. Saitta^{27,e}, M. Salomoni⁴⁸,
 D. Sanchez Gonzalo⁴⁵, C. Sanchez Gras³², R. Santacesaria³⁰, C. Santamarina Rios⁴⁶,
 M. Santimaria²³, E. Santovetti^{31,p}, D. Saranin⁸³, G. Sarpis⁵⁹, M. Sarpis⁷⁵, A. Sarti³⁰,
 C. Satriano^{30,o}, A. Satta³¹, M. Saur¹⁵, D. Savrina^{41,40}, H. Sazak⁹, L.G. Scantlebury Smead⁶³,
 S. Schael¹⁴, M. Schellenberg¹⁵, M. Schiller⁵⁹, H. Schindler⁴⁸, M. Schmelling¹⁶, B. Schmidt⁴⁸,
 O. Schneider⁴⁹, A. Schopper⁴⁸, M. Schubiger³², S. Schulte⁴⁹, M.H. Schune¹¹, R. Schwemmer⁴⁸,
 B. Sciascia²³, S. Sellam⁴⁶, A. Semennikov⁴¹, M. Senghi Soares³³, A. Sergi²⁴, N. Serra⁵⁰,
 L. Sestini²⁸, A. Seuthe¹⁵, P. Seyfert⁴⁸, Y. Shang⁵, D.M. Shangase⁸⁶, M. Shapkin⁴⁴,
 I. Shchemerov⁸³, L. Shchutska⁴⁹, T. Shears⁶⁰, L. Shekhtman^{43,v}, Z. Shen⁵, V. Shevchenko⁸¹,
 E.B. Shields^{26,j}, E. Shmanin⁸³, J.D. Shupperd⁶⁸, B.G. Siddi²¹, R. Silva Coutinho⁵⁰, G. Simi²⁸,
 S. Simone^{19,c}, N. Skidmore⁶², T. Skwarnicki⁶⁸, M.W. Slater⁵³, I. Slazyk^{21,f}, J.C. Smallwood⁶³,
 J.G. Smeaton⁵⁵, A. Smetkina⁴¹, E. Smith¹⁴, M. Smith⁶¹, A. Snoch³², M. Soares²⁰,
 L. Soares Lavra⁹, M.D. Sokoloff⁶⁵, F.J.P. Soler⁵⁹, A. Solovov³⁸, I. Solovyev³⁸,
 F.L. Souza De Almeida², B. Souza De Paula², B. Spaan¹⁵, E. Spadaro Norella^{25,i}, P. Spradlin⁵⁹,
 F. Stagni⁴⁸, M. Stahl⁶⁵, S. Stahl⁴⁸, P. Stefko⁴⁹, O. Steinkamp^{50,83}, O. Stenyakin⁴⁴, H. Stevens¹⁵,
 S. Stone⁶⁸, M.E. Stramaglia⁴⁹, M. Straticiu³⁷, D. Strelakina⁸³, F. Suljik⁶³, J. Sun²⁷, L. Sun⁷³,
 Y. Sun⁶⁶, P. Svihra⁶², P.N. Swallow⁵³, K. Swientek³⁴, A. Szabelski³⁶, T. Szumlak³⁴,
 M. Szymanski⁴⁸, S. Taneja⁶², F. Teubert⁴⁸, E. Thomas⁴⁸, K.A. Thomson⁶⁰, V. Tisserand⁹,
 S. T'Jampens⁸, M. Tobin⁴, L. Tomassetti^{21,f}, D. Torres Machado¹, D.Y. Tou¹³, M.T. Tran⁴⁹,
 E. Trifonova⁸³, C. Trippel⁴⁹, G. Tuci^{29,n}, A. Tully⁴⁹, N. Tuning^{32,48}, A. Ukleja³⁶,
 D.J. Unverzagt¹⁷, E. Ursov⁸³, A. Usachov³², A. Ustyuzhanin^{42,82}, U. Uwer¹⁷, A. Vagner⁸⁴,
 V. Vagnoni²⁰, A. Valassi⁴⁸, G. Valenti²⁰, N. Valls Canudas⁸⁵, M. van Beuzekom³²,
 M. Van Dijk⁴⁹, E. van Herwijnen⁸³, C.B. Van Hulse¹⁸, M. van Veghel⁷⁹, R. Vazquez Gomez⁴⁶,
 P. Vazquez Regueiro⁴⁶, C. Vázquez Sierra⁴⁸, S. Vecchi²¹, J.J. Velthuis⁵⁴, M. Veltri^{22,r},
 A. Venkateswaran⁶⁸, M. Veronesi³², M. Vesterinen⁵⁶, D. Vieira⁶⁵, M. Vieites Diaz⁴⁹,

H. Viemann⁷⁶, X. Vilasis-Cardona⁸⁵, E. Vilella Figueras⁶⁰, P. Vincent¹³, D. Vom Bruch¹⁰, A. Vorobyev³⁸, V. Vorobyev^{43,v}, N. Voropaev³⁸, R. Waldi⁷⁶, J. Walsh²⁹, C. Wang¹⁷, J. Wang⁵, J. Wang⁴, J. Wang³, J. Wang⁷³, M. Wang³, R. Wang⁵⁴, Y. Wang⁷, Z. Wang⁵⁰, Z. Wang³, H.M. Wark⁶⁰, N.K. Watson⁵³, S.G. Weber¹³, D. Websdale⁶¹, C. Weisser⁶⁴, B.D.C. Westhenry⁵⁴, D.J. White⁶², M. Whitehead⁵⁴, D. Wiedner¹⁵, G. Wilkinson⁶³, M. Wilkinson⁶⁸, I. Williams⁵⁵, M. Williams⁶⁴, M.R.J. Williams⁵⁸, F.F. Wilson⁵⁷, W. Wislicki³⁶, M. Witek³⁵, L. Witola¹⁷, G. Wormser¹¹, S.A. Wotton⁵⁵, H. Wu⁶⁸, K. Wyllie⁴⁸, Z. Xiang⁶, D. Xiao⁷, Y. Xie⁷, A. Xu⁵, J. Xu⁶, L. Xu³, M. Xu⁷, Q. Xu⁶, Z. Xu⁵, Z. Xu⁶, D. Yang³, S. Yang⁶, Y. Yang⁶, Z. Yang³, Z. Yang⁶⁶, Y. Yao⁶⁸, L.E. Yeomans⁶⁰, H. Yin⁷, J. Yu⁷¹, X. Yuan⁶⁸, O. Yushchenko⁴⁴, E. Zaffaroni⁴⁹, M. Zavertyaev^{16,u}, M. Zdybal³⁵, O. Zenaiev⁴⁸, M. Zeng³, D. Zhang⁷, L. Zhang³, S. Zhang⁵, Y. Zhang⁵, Y. Zhang⁶³, A. Zhelezov¹⁷, Y. Zheng⁶, X. Zhou⁶, Y. Zhou⁶, X. Zhu³, Z. Zhu⁶, V. Zhukov^{14,40}, J.B. Zonneveld⁵⁸, Q. Zou⁴, S. Zucchelli^{20,d}, D. Zuliani²⁸, G. Zunica⁶².

¹*Centro Brasileiro de Pesquisas Físicas (CBPF), Rio de Janeiro, Brazil*

²*Universidade Federal do Rio de Janeiro (UFRJ), Rio de Janeiro, Brazil*

³*Center for High Energy Physics, Tsinghua University, Beijing, China*

⁴*Institute Of High Energy Physics (IHEP), Beijing, China*

⁵*School of Physics State Key Laboratory of Nuclear Physics and Technology, Peking University, Beijing, China*

⁶*University of Chinese Academy of Sciences, Beijing, China*

⁷*Institute of Particle Physics, Central China Normal University, Wuhan, Hubei, China*

⁸*Univ. Savoie Mont Blanc, CNRS, IN2P3-LAPP, Annecy, France*

⁹*Université Clermont Auvergne, CNRS/IN2P3, LPC, Clermont-Ferrand, France*

¹⁰*Aix Marseille Univ, CNRS/IN2P3, CPPM, Marseille, France*

¹¹*Université Paris-Saclay, CNRS/IN2P3, IJCLab, Orsay, France*

¹²*Laboratoire Leprince-Ringuet, CNRS/IN2P3, Ecole Polytechnique, Institut Polytechnique de Paris, Palaiseau, France*

¹³*LPNHE, Sorbonne Université, Paris Diderot Sorbonne Paris Cité, CNRS/IN2P3, Paris, France*

¹⁴*I. Physikalisches Institut, RWTH Aachen University, Aachen, Germany*

¹⁵*Fakultät Physik, Technische Universität Dortmund, Dortmund, Germany*

¹⁶*Max-Planck-Institut für Kernphysik (MPIK), Heidelberg, Germany*

¹⁷*Physikalisches Institut, Ruprecht-Karls-Universität Heidelberg, Heidelberg, Germany*

¹⁸*School of Physics, University College Dublin, Dublin, Ireland*

¹⁹*INFN Sezione di Bari, Bari, Italy*

²⁰*INFN Sezione di Bologna, Bologna, Italy*

²¹*INFN Sezione di Ferrara, Ferrara, Italy*

²²*INFN Sezione di Firenze, Firenze, Italy*

²³*INFN Laboratori Nazionali di Frascati, Frascati, Italy*

²⁴*INFN Sezione di Genova, Genova, Italy*

²⁵*INFN Sezione di Milano, Milano, Italy*

²⁶*INFN Sezione di Milano-Bicocca, Milano, Italy*

²⁷*INFN Sezione di Cagliari, Monserrato, Italy*

²⁸*Università degli Studi di Padova, Università e INFN, Padova, Padova, Italy*

²⁹*INFN Sezione di Pisa, Pisa, Italy*

³⁰*INFN Sezione di Roma La Sapienza, Roma, Italy*

³¹*INFN Sezione di Roma Tor Vergata, Roma, Italy*

³²*Nikhef National Institute for Subatomic Physics, Amsterdam, Netherlands*

³³*Nikhef National Institute for Subatomic Physics and VU University Amsterdam, Amsterdam, Netherlands*

³⁴*AGH - University of Science and Technology, Faculty of Physics and Applied Computer Science, Kraków, Poland*

³⁵*Henryk Niewodniczanski Institute of Nuclear Physics Polish Academy of Sciences, Kraków, Poland*

³⁶*National Center for Nuclear Research (NCBJ), Warsaw, Poland*

³⁷*Horia Hulubei National Institute of Physics and Nuclear Engineering, Bucharest-Magurele, Romania*

³⁸*Petersburg Nuclear Physics Institute NRC Kurchatov Institute (PNPI NRC KI), Gatchina, Russia*

- ³⁹*Institute for Nuclear Research of the Russian Academy of Sciences (INR RAS), Moscow, Russia*
- ⁴⁰*Institute of Nuclear Physics, Moscow State University (SINP MSU), Moscow, Russia*
- ⁴¹*Institute of Theoretical and Experimental Physics NRC Kurchatov Institute (ITEP NRC KI), Moscow, Russia*
- ⁴²*Yandex School of Data Analysis, Moscow, Russia*
- ⁴³*Budker Institute of Nuclear Physics (SB RAS), Novosibirsk, Russia*
- ⁴⁴*Institute for High Energy Physics NRC Kurchatov Institute (IHEP NRC KI), Protvino, Russia, Protvino, Russia*
- ⁴⁵*ICCUB, Universitat de Barcelona, Barcelona, Spain*
- ⁴⁶*Instituto Galego de Física de Altas Enerxías (IGFAE), Universidade de Santiago de Compostela, Santiago de Compostela, Spain*
- ⁴⁷*Instituto de Física Corpuscular, Centro Mixto Universidad de Valencia - CSIC, Valencia, Spain*
- ⁴⁸*European Organization for Nuclear Research (CERN), Geneva, Switzerland*
- ⁴⁹*Institute of Physics, Ecole Polytechnique Fédérale de Lausanne (EPFL), Lausanne, Switzerland*
- ⁵⁰*Physik-Institut, Universität Zürich, Zürich, Switzerland*
- ⁵¹*NSC Kharkiv Institute of Physics and Technology (NSC KIPT), Kharkiv, Ukraine*
- ⁵²*Institute for Nuclear Research of the National Academy of Sciences (KINR), Kyiv, Ukraine*
- ⁵³*University of Birmingham, Birmingham, United Kingdom*
- ⁵⁴*H.H. Wills Physics Laboratory, University of Bristol, Bristol, United Kingdom*
- ⁵⁵*Cavendish Laboratory, University of Cambridge, Cambridge, United Kingdom*
- ⁵⁶*Department of Physics, University of Warwick, Coventry, United Kingdom*
- ⁵⁷*STFC Rutherford Appleton Laboratory, Didcot, United Kingdom*
- ⁵⁸*School of Physics and Astronomy, University of Edinburgh, Edinburgh, United Kingdom*
- ⁵⁹*School of Physics and Astronomy, University of Glasgow, Glasgow, United Kingdom*
- ⁶⁰*Oliver Lodge Laboratory, University of Liverpool, Liverpool, United Kingdom*
- ⁶¹*Imperial College London, London, United Kingdom*
- ⁶²*Department of Physics and Astronomy, University of Manchester, Manchester, United Kingdom*
- ⁶³*Department of Physics, University of Oxford, Oxford, United Kingdom*
- ⁶⁴*Massachusetts Institute of Technology, Cambridge, MA, United States*
- ⁶⁵*University of Cincinnati, Cincinnati, OH, United States*
- ⁶⁶*University of Maryland, College Park, MD, United States*
- ⁶⁷*Los Alamos National Laboratory (LANL), Los Alamos, United States*
- ⁶⁸*Syracuse University, Syracuse, NY, United States*
- ⁶⁹*School of Physics and Astronomy, Monash University, Melbourne, Australia, associated to ⁵⁶*
- ⁷⁰*Pontifícia Universidade Católica do Rio de Janeiro (PUC-Rio), Rio de Janeiro, Brazil, associated to ²*
- ⁷¹*Physics and Micro Electronic College, Hunan University, Changsha City, China, associated to ⁷*
- ⁷²*Guangdong Provincial Key Laboratory of Nuclear Science, Institute of Quantum Matter, South China Normal University, Guangzhou, China, associated to ³*
- ⁷³*School of Physics and Technology, Wuhan University, Wuhan, China, associated to ³*
- ⁷⁴*Departamento de Física, Universidad Nacional de Colombia, Bogota, Colombia, associated to ¹³*
- ⁷⁵*Universität Bonn - Helmholtz-Institut für Strahlen und Kernphysik, Bonn, Germany, associated to ¹⁷*
- ⁷⁶*Institut für Physik, Universität Rostock, Rostock, Germany, associated to ¹⁷*
- ⁷⁷*Eotvos Lorand University, Budapest, Hungary, associated to ⁴⁸*
- ⁷⁸*INFN Sezione di Perugia, Perugia, Italy, associated to ²¹*
- ⁷⁹*Van Swinderen Institute, University of Groningen, Groningen, Netherlands, associated to ³²*
- ⁸⁰*Universiteit Maastricht, Maastricht, Netherlands, associated to ³²*
- ⁸¹*National Research Centre Kurchatov Institute, Moscow, Russia, associated to ⁴¹*
- ⁸²*National Research University Higher School of Economics, Moscow, Russia, associated to ⁴²*
- ⁸³*National University of Science and Technology "MISIS", Moscow, Russia, associated to ⁴¹*
- ⁸⁴*National Research Tomsk Polytechnic University, Tomsk, Russia, associated to ⁴¹*
- ⁸⁵*DS4DS, La Salle, Universitat Ramon Llull, Barcelona, Spain, associated to ⁴⁵*
- ⁸⁶*University of Michigan, Ann Arbor, United States, associated to ⁶⁸*

^a*Universidade Federal do Triângulo Mineiro (UFTM), Uberaba-MG, Brazil*

^b*Hangzhou Institute for Advanced Study, UCAS, Hangzhou, China*

^c*Università di Bari, Bari, Italy*

^d*Università di Bologna, Bologna, Italy*

- ^e *Università di Cagliari, Cagliari, Italy*
- ^f *Università di Ferrara, Ferrara, Italy*
- ^g *Università di Firenze, Firenze, Italy*
- ^h *Università di Genova, Genova, Italy*
- ⁱ *Università degli Studi di Milano, Milano, Italy*
- ^j *Università di Milano Bicocca, Milano, Italy*
- ^k *Università di Modena e Reggio Emilia, Modena, Italy*
- ^l *Università di Padova, Padova, Italy*
- ^m *Scuola Normale Superiore, Pisa, Italy*
- ⁿ *Università di Pisa, Pisa, Italy*
- ^o *Università della Basilicata, Potenza, Italy*
- ^p *Università di Roma Tor Vergata, Roma, Italy*
- ^q *Università di Siena, Siena, Italy*
- ^r *Università di Urbino, Urbino, Italy*
- ^s *MSU - Iligan Institute of Technology (MSU-IIT), Iligan, Philippines*
- ^t *AGH - University of Science and Technology, Faculty of Computer Science, Electronics and Telecommunications, Kraków, Poland*
- ^u *P.N. Lebedev Physical Institute, Russian Academy of Science (LPI RAS), Moscow, Russia*
- ^v *Novosibirsk State University, Novosibirsk, Russia*
- ^w *Department of Physics and Astronomy, Uppsala University, Uppsala, Sweden*
- ^x *Hanoi University of Science, Hanoi, Vietnam*